

Mechanical Squeezed-Fock Gravimeter

Rozhin Yousefjani^{1,*} and Saif Al-Kuwari¹

¹*Qatar Center for Quantum Computing, College of Science and Engineering, Hamad Bin Khalifa University, Doha, Qatar*

Levitated mechanical systems are promising candidates for quantum gravimetry, as gravity couples directly to their center-of-mass motion, enabling the large mass of a mesoscopic particle to serve as a sensing resource. In this paper, we propose a mechanical squeezed-Fock qubit gravimeter using a Duffing oscillator that is driven by a detuned two-phonon pump. In the squeezed-Fock basis, the gravitational force couples to the anti-squeezed quadrature, which enhances the gravity-induced transition rate while preserving the direct mass scaling of the mechanical force coupling. We show that sensitivity improves with reduced effective qubit splitting that is controlled by squeezing parameter, and the Duffing nonlinearity. We further analyze mechanical damping and show that squeezing converts ordinary dissipation into anisotropic qubit noise, setting a practical trade-off between signal amplification and decoherence rate. These results identify the mechanical squeezed-Fock qubit as a new platform for quantum-enhanced gravimetry.

I. INTRODUCTION

Precision measurements of gravitational acceleration g lie at the intersection of fundamental physics and applied science, underpinning applications that range from underground mapping and geophysical surveying [1–4] to inertial navigation [5] and tests of the equivalence principle [6, 7]. The prevailing technology in quantum gravimetry relies on free-falling cold-atom interferometers, which encode the gravitational phase into the coherence of atomic matter waves [8–11]. These systems have reached sub- $\mu\text{Gal}/\sqrt{\text{Hz}}$ ($1\mu\text{Gal} = 10\text{nm/s}^2$) sensitivities [12–15], but their sensitivity scales with the interrogation arm length and they require free-fall operation [10, 16], which places stringent demands on vibration isolation, footprint, and device complexity [10, 14, 17–19]. Identifying platforms that deliver high sensitivity without relying on free-fall, and whose gravitational response grows with a resource controllable in the laboratory, is therefore a key challenge for next-generation compact gravimeters.

Levitated mesoscopic particles have emerged as a compelling alternative [20–22]. The absence of mechanical clamping removes the dominant loss channel of conventional resonators, enabling quality factors as high as $Q \sim 10^9$ under high vacuum [23]. The gravitational response of a levitated object is proportional to its mass m , providing a susceptibility that scales as \sqrt{m} orders of magnitude larger than for atomic sensors [20, 24]. The most natural approach is to encode g directly in the center-of-mass (CM) motion and read out the resulting phase or population [23, 25–30]. However, the CM mode of a harmonic oscillator has an equally spaced spectrum with no metrological advantage specific to a particular pair of levels. To solve this issue, conventional levitated-particle gravimetry has therefore coupled the mechanical mode to other strongly nonlinear quantum systems, such as an electron-spin qubit [31, 32] or an optical cavity [33]. However, this approach has fundamental limitations. The coupling between the CM mode and the auxiliary system scales as

$1/\sqrt{m}$ [34, 35], exactly canceling the \sqrt{m} enhancement from the particle’s mass. As a result, the sensitivity of hybrid gravimeters is mass-independent [31–33].

A possible solution is to encode the qubit directly in the CM mode, established based on quantized motional modes, provided that the mechanical spectrum is made sufficiently anharmonic [36]. Introducing Duffing nonlinearity splits the ladder of Fock states and allows the two lowest levels to be addressed selectively [37–39]. This *mechanical qubit* (MQ) [36, 37, 40–43] has recently been demonstrated experimentally [44], establishing phononic two-level systems as a realistic platform for quantum information [45] and quantum sensing [24, 37, 46]. Since the MQ couples to gravity directly through its CM displacement, with no auxiliary system involved, the mass enhancement is fully preserved. Huo *et al.* [24] recently exploited this insight to propose a mass-enhanced quantum gravimeter based on MQs and their cat-state counterparts. Despite this progress, MQ implementations remain constrained by a central physical bottleneck: nanomechanical resonators typically exhibit weak intrinsic nonlinearities and limited anharmonicity, making robust state preparation and coherent control challenging [29, 36–38, 44]. A complementary line of development is to map the original Fock ladder into a *squeezed-Fock ladder* whose effective anharmonicity is exponentially enhanced by e^{4r} , where r is the squeezing parameter [46]. The resulting *mechanical squeezed-Fock qubit* (MSFQ) allows a mechanical qubit to be encoded even when the intrinsic nonlinearity is weak [46].

In this paper, we propose and analyze the mechanical squeezed-Fock gravimeter, a new sensing approach that combines the direct mass advantage of the MQ architecture with the exponential signal amplification of the squeezed-Fock states. We drive the CM mode with a *detuned* two-phonon pump and employ a Rabi-based interrogation protocol sensitive to the static gravity force. Gravity couples to the anti-squeezed quadrature of the CM mode with an amplitude $\propto e^r$, producing a gravity-induced coupling that exceeds its MQ counterpart [24] by e^r . In our protocol, effective qubit splitting can be fully controlled by adjusting the Duffing nonlinearity as well as the squeezing parameter, which results in

* ryousefjani@hbku.edu.qa

extending the coherent interrogation time and further improving sensitivity. Using quantum estimation theory [47–49], we derive the exact quantum Fisher information (QFI) and show that it is saturated by a simple squeezed-Fock population measurement. We further analyze the effect of mechanical damping and show that squeezing transforms ordinary damping into anisotropic qubit noise in the squeezed-qubit subspace. As a result, the standard population measurement is no longer optimal, and the optimized readout is obtained by measuring along the symmetric-logarithmic-derivative direction. The performance of the gravimeter is governed by a competition between coherent Rabi precession and the anisotropic decay channel. We determine the practical operating window of the sensor and show that squeezing is beneficial as long as the enhanced decoherence rate remains comparable to the coherent qubit dynamics.

II. QUANTUM ESTIMATION THEORY

For an unknown parameter g that is encoded in the sensor state $\rho_g(t)$, a measurement, represented by a POVM $\{\Pi_x\}$, gives the outcome probabilities as $p(x|g)=\text{Tr}[\rho_g(t)\Pi_x]$. For this fixed measurement, the classical Fisher information (CFI) is $\mathcal{F}_C(g)=\sum_x[\partial_g p(x|g)]^2/p(x|g)$, with zero-probability outcomes omitted. For ν independent repetitions, any unbiased estimator satisfies $\delta g \geq 1/\sqrt{\nu\mathcal{F}_C(g)}$. Optimizing over all POVMs gives the QFI, $\mathcal{F}_Q(g)=\max_{\{\Pi_x\}}\mathcal{F}_C(g)$. The corresponding quantum Cramér–Rao bound is $\delta g \geq 1/\sqrt{\nu\mathcal{F}_Q(g)}$. The QFI can be written in terms of the SLD \hat{L}_g , defined implicitly by $\partial_g \rho_g=(\rho_g \hat{L}_g + \hat{L}_g \rho_g)/2$. It is then $\mathcal{F}_Q(g)=\text{Tr}[\rho_g \hat{L}_g^2]=\text{Tr}[(\partial_g \rho_g) \hat{L}_g]$. The locally optimal measurement is the projective measurement in the eigenbasis of \hat{L}_g . For a pure state $\rho_g=|\psi_g\rangle\langle\psi_g|$, the QFI reduces to [50]

$$\mathcal{F}_Q(g) = 4 \left[\langle \partial_g \psi_g | \partial_g \psi_g \rangle - |\langle \psi_g | \partial_g \psi_g \rangle|^2 \right]. \quad (1)$$

For a qubit mixed state $\rho_g=(\mathbb{I}+\mathbf{v}\cdot\boldsymbol{\sigma})/2$, one has $\mathcal{F}_Q(g)=|\partial_g \mathbf{v}|^2+(\mathbf{v}\cdot\partial_g \mathbf{v})^2/(1-|\mathbf{v}|^2)$ for $|\mathbf{v}|<1$.

III. MODEL

The MQ considered here is made from the CM motion of a levitated mesoscopic particle along the gravitational direction with Duffing nonlinearity of strength D . The free Hamiltonian of this mechanical mode is written as

$$\hat{H}=\hbar\omega\hat{a}^\dagger\hat{a}-\hbar D\hat{a}^\dagger\hat{a}^\dagger\hat{a}\hat{a}, \quad (2)$$

where \hat{a} (\hat{a}^\dagger) is the annihilation (creation) operator of the CM mode with frequency ω . The corresponding eigenenergies of this system are $E_n=n\hbar\omega-n(n-1)\hbar D$. Clearly, unlike a purely harmonic oscillator, the level spacing is no longer uniform. In particular, the transition frequency between the Fock states $|1\rangle$ and $|2\rangle$ differs from that between $|0\rangle$ and $|1\rangle$ by the anharmonicity $-2\hbar D$. This anharmonicity is the key ingredient that allows one to interpret the mechanical

oscillator as an effective qubit rather than as a fully harmonic mode. A MQ is obtained when the system dynamics is effectively restricted to the two-dimensional subspace spanned by the lowest two eigenstates, namely the ground state $|0\rangle$ and the first excited state $|1\rangle$. Physically, this requires that all external perturbations, driving amplitudes, and dissipative broadenings remain much smaller than the anharmonicity value, so that leakage to higher states is suppressed.

To create a squeezed-Fock spectrum following [46], we drive our Duffing oscillator with a *detuned* two-phonon pump of frequency $2\omega_p$ with phase θ and amplitude A_p . This reshapes the CM spectrum into a squeezed and more strongly anharmonic one, such that the effective qubit subspace is no longer formed by the bare Fock states $\{|0\rangle,|1\rangle\}$, but by the two lowest squeezed-Fock states. The Hamiltonian of the Duffing oscillator under detuned drive reads

$$\begin{aligned} \hat{H} &= \hbar\omega\hat{a}^\dagger\hat{a}-\hbar D\hat{a}^\dagger\hat{a}^\dagger\hat{a}\hat{a} \\ &+ \frac{\hbar A_p}{2} \left(e^{-i(2\omega_p t+\theta)}\hat{a}^2+e^{i(2\omega_p t+\theta)}\hat{a}^{\dagger 2} \right). \end{aligned} \quad (3)$$

In the frame rotating at ω_p via $\hat{U}_0(t)=e^{-i\omega_p\hat{a}^\dagger\hat{a}t}$, one has

$$\hat{H}_{\text{rot}}=\hbar\delta\hat{a}^\dagger\hat{a}-\hbar D\hat{a}^\dagger\hat{a}^\dagger\hat{a}\hat{a}+\frac{\hbar A_p}{2} \left(e^{-i\theta}\hat{a}^2+e^{i\theta}\hat{a}^{\dagger 2} \right) \quad (4)$$

where $\delta=\omega-\omega_p$ is the detuning. Using the Bogoliubov transformation $\hat{b}=\hat{S}\hat{a}\hat{S}^\dagger$ with the squeezing operator $\hat{S}=\exp(r^*\hat{a}^2/2+r\hat{a}^{\dagger 2}/2)$ and squeezing parameter r that satisfies $\tanh(2r)=A_p/\delta$ one can obtain the new mechanical mode $\hat{b}=\cosh r\hat{a}+e^{i\theta}\sinh r\hat{a}^\dagger$. Equivalently one has $\hat{a}=\cosh r\hat{b}-e^{i\theta}\sinh r\hat{b}^\dagger$. Under the rotating-wave approximation (RWA), the Hamiltonian (4) is transformed into an effective form as (see Appendix A),

$$\hat{H}_{\text{eff}}\simeq\hbar\omega_b\hat{b}^\dagger\hat{b}-\hbar U_b\hat{b}^\dagger\hat{b}^\dagger\hat{b}\hat{b}, \quad (5)$$

with $\omega_b=\sqrt{\delta^2-A_p^2}-D(8\cosh^2 r\sinh^2 r+4\sinh^4 r)$, and $U_b=\frac{D}{4}[3\cosh(4r)+1]$. The minus sign in front of the quartic term reflects the sign of the Duffing nonlinearity in the levitated mechanical platform. The shape of ω_b obligates us to determine the boundary at which the qubit gap closes, namely $\omega_b=0$. As such, we introduce $D_{\text{crit}}=\sqrt{\delta^2-A_p^2}/(8\cosh^2 r\sinh^2 r+4\sinh^4 r)$ and define the physically allowed range of the Duffing parameter $D<D_{\text{crit}}$ for which ω_b does not vanish. Besides this, the RWA validity limits the accessible range of D/D_{crit} . Beyond this region, the effective Hamiltonian (5) is no longer a reliable description of the dynamics. See Appendix A for a detailed discussion.

IV. QUANTUM GRAVIMETER

In the mechanical-mode description, gravity appears as a static linear force, $(mg-F)x_0(\hat{a}+\hat{a}^\dagger)$. The detuned two-phonon pump defines a squeezed-Fock basis in which the displacement quadrature coupled to gravity is rescaled by e^r ,

provided that the pump phase θ is chosen such that gravity couples to the anti-squeezed quadrature. Selecting $\theta=\pi$, results in $\hat{a}+\hat{a}^\dagger=e^r(\hat{b}+\hat{b}^\dagger)$, and hence, $\hat{H}_g^s=G(\hat{b}+\hat{b}^\dagger)$, with $G=e^r(mg-F)x_0$. Here, F is a static compensation force applied opposite to gravity and chosen such that $G\ll 2U_b$, which keeps the sensor near its optimal working point and suppresses leakage out of the squeezed-qubit subspace. The quantity $x_0=\sqrt{\hbar/2m\omega}$ is the zero-point fluctuation amplitude. In the MSFQ framework, where $\hat{b}+\hat{b}^\dagger\rightarrow\hat{\sigma}_x$, the effective gravimeter Hamiltonian reads

$$\hat{H}_{\text{eff}}^s=\frac{\hbar\omega_b}{2}\hat{\sigma}_z+\frac{\hbar\Omega_g^s}{2}\hat{\sigma}_x, \quad (6)$$

with the gravity-induced coupling $\Omega_g^s=2e^r\frac{(mg-F)x_0}{\hbar}$. Obviously, the static gravitational force is enhanced by a factor e^r at the Hamiltonian level, which makes the qubit populations more sensitive to small changes in g . This enhancement does not come from adding an auxiliary sensor or increasing the particle mass. It comes from reshaping the mechanical mode itself.

Initializing the sensor in the ground squeezed state, $|\psi(0)\rangle=|0\rangle_s$, results in $|\psi(t)\rangle=e^{-i\hat{H}_{\text{eff}}^s t/\hbar}|0\rangle_s=\alpha(t)|0\rangle_s+\beta(t)|1\rangle_s$, where $\alpha(t)=\cos\left(\frac{\omega_R t}{2}\right)+i\frac{\omega_b}{\omega_R}\sin\left(\frac{\omega_R t}{2}\right)$, and $\beta(t)=-i\frac{\Omega_g^s}{\omega_R}\sin\left(\frac{\omega_R t}{2}\right)$ for $\omega_R=\sqrt{\omega_b^2+\Omega_g^s{}^2}$ as the generalized Rabi frequency. The exact QFI for estimating g from this state is derived in the Appendix B. In the weak-force regime, namely $\Omega_g^s\ll\omega_b$, the exact result reduces to

$$\mathcal{F}_Q(g,t)\simeq\frac{8me^{2r}}{\hbar\omega\omega_b^2}\sin^2\left(\frac{\omega_b t}{2}\right). \quad (7)$$

which peaks at $\omega_b t=(2\ell+1)\pi$, with integer ℓ . The first optimal interrogation time is $t_{\text{opt}}=\frac{\pi}{\omega_b}$ for which

$$\mathcal{F}_{Q,\text{max}}(g)\simeq\frac{8me^{2r}}{\hbar\omega\omega_b^2}. \quad (8)$$

If each run takes an interrogation time t and the total averaging time is T , then $\nu=T/t$ and the time-normalized sensitivity obeys

$$\sqrt{T}\delta g_{\text{opt}}^s\simeq\sqrt{\frac{\pi\hbar\omega\omega_b}{8me^{2r}}} \quad (9)$$

at $t=t_{\text{opt}}$. To approach this bound, one can measure the excited squeezed-Fock population, $\hat{O}_s=|1\rangle_{\text{ss}}\langle 1|$. The corresponding probability is $P_1(t)=\frac{\Omega_g^s{}^2}{\omega_R^2}\sin^2\left(\frac{\omega_R t}{2}\right)$. The exact CFI associated with the binary outcomes $P_1(t)$ and $1-P_1(t)$ is given in the Appendix B. In the same weak-force regime, it reduces to

$$\mathcal{F}_C(g,t)\simeq\frac{8me^{2r}}{\hbar\omega\omega_b^2}\sin^2\left(\frac{\omega_b t}{2}\right)=\mathcal{F}_Q(g,t). \quad (10)$$

Therefore, the excited-state occupation measurement is optimal in the weak-force regime.

Apart from m and ω , the precision is governed most directly by two effective quantities: the squeezing parameter r and the

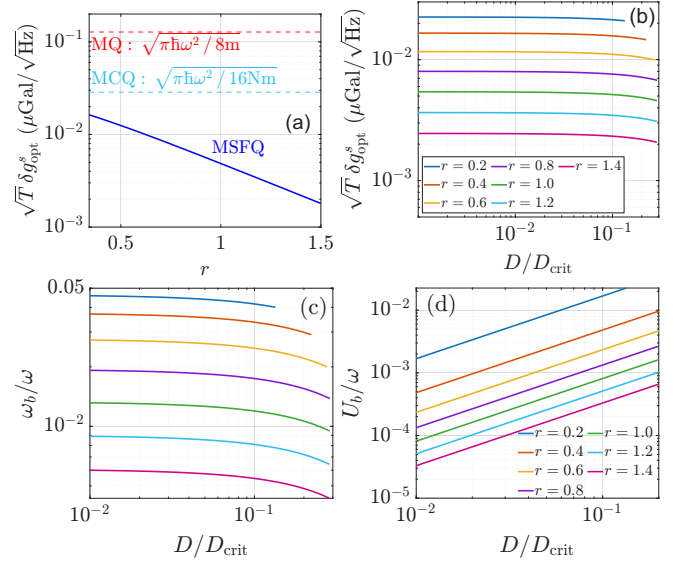


FIG. 1. Coherent performance of the MSFQ gravimeter. (a) Time-normalized sensitivity $\sqrt{T}\delta g_{\text{opt}}^s$ as a function of r at fixed $D/D_{\text{crit}}=0.2$. The horizontal lines mark the MQ sensitivity $\sqrt{\pi\hbar\omega^2/8m}$ and the MCQ sensitivity $\sqrt{\pi\hbar\omega^2/16mN}$ for $N=10$ reported in Ref. [24]. (b) $\sqrt{T}\delta g_{\text{opt}}^s$ as a function of D/D_{crit} for various r 's. (c) Qubit frequency ω_b/ω as a function of D/D_{crit} for the same values of r as in panel (b). (d) Effective anharmonicity U_b/ω as a function of D/D_{crit} for various r 's. In both panels, each curve is shown only within the RWA-valid region (see Appendix A). The physical parameters are $m=10^{-9}$ kg and $\omega/2\pi=1$ kHz, with $\delta/\omega=0.05$ throughout.

effective qubit frequency ω_b . While r is only controlled by the pump ratio A_p/δ , the frequency ω_b is jointly controlled by δ , A_p/δ , and D/D_{crit} . Obviously, the sensitivity is improved by increasing the Hamiltonian-level signal enhancement e^r and by reducing ω_b , but only within a regime where the interrogation time remains finite, and the RWA is valid, see Appendix A. Fig. 1 summarizes the coherent operating principle of the MSFQ gravimeter. Fig. 1(a) shows the time-normalized sensitivity $\sqrt{T}\delta g_{\text{opt}}^s$ as a function of the squeezing parameter r at fixed $D/D_{\text{crit}}=0.2$. Obviously $\sqrt{T}\delta g_{\text{opt}}^s$ decreases monotonically with r , reflecting the exponential enhancement e^r of the gravity-induced coupling at the Hamiltonian level. For sufficiently large r , MSFQ suppresses both MQ benchmark $\sqrt{\pi\hbar\omega^2/8m}$ and MCQ benchmark $\sqrt{\pi\hbar\omega^2/16mN}$ with $N=10$, reported in Ref. [24], demonstrating that squeezing alone is sufficient to achieve a competitive sensitivity. Fig. 1(b) shows the sensitivity as a function of D/D_{crit} for fixed values of $r\in\{0.2,\dots,1.4\}$. Two effects are simultaneously visible. First, for any fixed r , the sensitivity improves monotonically as D/D_{crit} increases, because ω_b decreases and the coherent bound tightens accordingly. Second, at any fixed D/D_{crit} , increasing r shifts the entire curve downward by the exponential factor e^{-r} , confirming that squeezing is the dominant resource. The valid range of D/D_{crit} shrinks with increasing r . Figs 1(c) and (d) show, respectively, the squeezed qubit frequency ω_b/ω and the effective anharmonicity U_b/ω as functions of D/D_{crit} for various r 's. For any

fixed r , increasing D/D_{crit} simultaneously reduces ω_b/ω and raises U_b/ω , since both quantities are controlled by duffing parameter. Larger r shifts the ω_b/ω curves in panel (c) downward and the U_b/ω curves in panel (d) upward, amplifying both effects simultaneously; it also compresses the RWA-valid range to smaller D/D_{crit} . This joint behavior is doubly favorable: a smaller ω_b lengthens the optimal interrogation time $t_{\text{opt}} = \pi/\omega_b$ and tightens the coherent sensitivity bound, while a larger U_b exponentially increases the anharmonic protection of the squeezed-qubit subspace and suppresses leakage to higher squeezed-Fock levels.

V. EFFECT OF DECOHERENCE ON QUANTUM GRAVIMETER

The ideal results above assume that the MSFQ evolves coherently. We now include the dominant mechanical damping channel and derive the corresponding gravimetric sensitivity. In the laboratory frame, zero-temperature mechanical damping is described by [51–55]

$$\dot{\rho} = -\frac{i}{\hbar}[\hat{H}, \rho] + \frac{\gamma_0}{2}\mathcal{D}_{\hat{a}, \hat{a}^\dagger}[\rho], \quad \mathcal{D}_{\hat{A}, \hat{B}}[\rho] = 2\hat{A}\rho\hat{B} - \hat{B}\hat{A}\rho - \rho\hat{B}\hat{A}, \quad (11)$$

where γ_0 is the mechanical energy-relaxation rate. Using the Bogoliubov transformation maps and projecting onto the squeezed-qubit subspace $\{|0\rangle_s, |1\rangle_s\}$, results in the effective jump operator as $\hat{L}_s = \cosh r \hat{\sigma}_- + \sinh r \hat{\sigma}_+$. Then decoherent squeezed-qubit gravimeter is governed by

$$\dot{\rho} = -\frac{i}{2}[\hat{H}, \rho] + \frac{\gamma_0}{2}\mathcal{D}_{\hat{L}_s, \hat{L}_s^\dagger}[\rho]. \quad (12)$$

The Bloch vector $\mathbf{v} = (x, y, z)^T$ corresponding to ρ evolves as

$$\dot{\mathbf{v}} = \mathbf{A}(\Omega)\mathbf{v} + \mathbf{b}, \quad (13)$$

with the drift matrix

$$\mathbf{A} = \begin{pmatrix} -\Gamma_x & \omega_b & 0 \\ -\omega_b & -\Gamma_y & \Omega_g^s \\ 0 & -\Omega_g^s & -\Gamma_z \end{pmatrix}, \quad \mathbf{b} = \begin{pmatrix} 0 \\ 0 \\ -\gamma_0 \end{pmatrix}, \quad (14)$$

and the three anisotropic decoherence rates

$$\Gamma_x = \frac{\gamma_0}{2}e^{-2r}, \quad \Gamma_y = \frac{\gamma_0}{2}e^{2r}, \quad \Gamma_z = \gamma_0 \cosh(2r). \quad (15)$$

Clearly, the same squeezing that amplifies the gravitational signal also anisotropically amplifies the noise. The QFI is then

$$\mathcal{F}_Q^{\text{dec}}(g) = \kappa_g^2 \left[|\mathbf{u}|^2 + \frac{(\mathbf{v} \cdot \mathbf{u})^2}{1 - |\mathbf{v}|^2} \right], \quad \kappa_g^2 = \frac{2me^{2r}}{\hbar\omega}, \quad (16)$$

where $\mathbf{u} = \partial_\Omega \mathbf{v}$ is the sensitivity vector satisfying the same drift matrix, sourced by $\partial_\Omega \mathbf{A}$ (see Appendix C). The anisotropic damping redistributes information about g among all three Bloch-vector components. Therefore, the standard population measurement is no longer optimal in the presence of decoherence. The optimized readout, obtained by measuring along the symmetric-logarithmic-derivative direction \mathbf{n}_{opt} , extracts

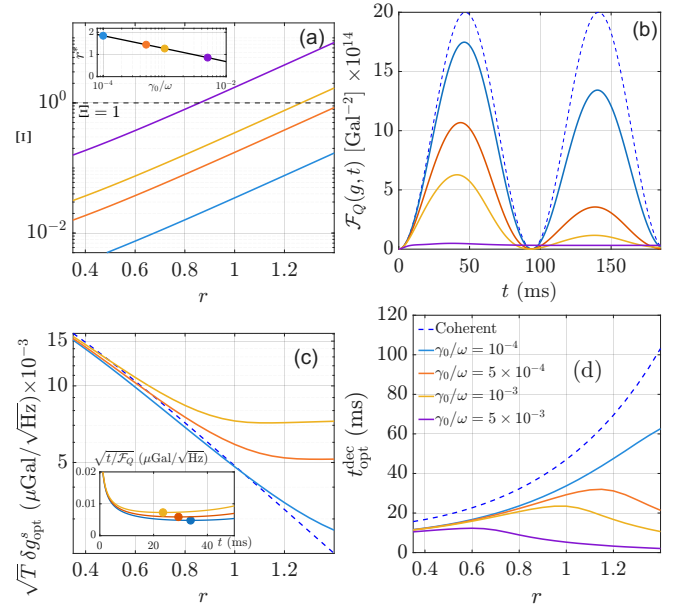


FIG. 2. Decoherent performance of the MSFQ gravimeter, for $m=10^{-9}$ kg, $\omega/2\pi=1$ kHz, and $\delta/\omega=0.05$ throughout. (a) Competition ratio $\Xi \equiv \Gamma_{\text{eff}}/\omega_b$ as a function of r at fixed $D/D_{\text{crit}}=0.2$, for various γ_0 's. The dashed line $\Xi=1$ marks the crossover between the coherent ($\Xi \ll 1$) and decoherent ($\Xi \gg 1$) regimes. (b) QFI $\mathcal{F}_Q(g, t)$ as a function of time at fixed $D/D_{\text{crit}}=0.2$ and $r=1$, for various γ_0 's and the coherent reference ($\gamma_0=0$, dashed). (c) Optimized sensitivity $\sqrt{T} \delta g_{\text{opt}}^s$ as a function of r at fixed $D/D_{\text{crit}}=0.2$, evaluated at the decoherence-limited interrogation time $t_{\text{opt}}^{\text{dec}} \equiv \arg \min_t \sqrt{t/\mathcal{F}_Q(g, t)}$ shown as markers in the inset. (d) Decoherence-limited optimal interrogation time $t_{\text{opt}}^{\text{dec}}$ as a function of r at fixed $D/D_{\text{crit}}=0.2$, for various γ_0 's with the coherent reference $t_{\text{opt}} = \pi/\omega_b$ (dashed).

the full information stored in the Bloch vector. As a result, the optimized CFI coincides with the QFI at the chosen operating point (see Appendix C and Fig. C1).

The decoherent QFI is governed by the prefactor κ_g^2 and by the sensitivity vector $\mathbf{u}(t) = \partial_\Omega \mathbf{v}(t)$, whose magnitude and orientation are set by the competition between coherent Rabi precession at frequency ω_b and the anisotropic decay channel. This competition is governed by

$$\Xi \equiv \frac{\Gamma_{\text{eff}}}{\omega_b}, \quad \Gamma_{\text{eff}} \approx \frac{\gamma_0}{2}e^{2r}, \quad (17)$$

where Γ_{eff} is set by the dominant decoherence rate Γ_y . Fig. 2(a) shows Ξ as a function of r at fixed $D/D_{\text{crit}}=0.2$, for four values of γ_0/ω . For any fixed γ_0 , Ξ grows with r exponentially. Each curve crosses the threshold $\Xi=1$ at a squeezing value $r^*(\gamma_0)$ that shifts to smaller r as γ_0 increases, see the inset of Fig. 2(a). Below this threshold, the qubit completes a Rabi oscillation before decoherence acts, and the coherent regime is recovered; above it, the sensor relaxes before the gravity signal is encoded, as it can be seen from Fig. 2(b). This panel reports the QFI dynamics at fixed $r=1$ and $D/D_{\text{crit}}=0.2$ for the same set of γ_0/ω values, together with the coherent reference. In the coherent limit ($\gamma_0=0$),

the QFI oscillates periodically with maxima at odd multiples of $t_{\text{opt}}=\pi/\omega_b$, as predicted by Eq. (7). For $\gamma_0/\omega=10^{-4}$, the system lies below $\Xi=1$ at $r=1$ and the envelope of the oscillations is only weakly damped, so the first peak closely approaches the coherent value. As γ_0 increases and Ξ exceeds unity, the QFI peak is progressively suppressed and displaced to earlier times, narrowing the window of useful sensing. See the results for $\gamma_0/\omega=5 \times 10^{-3}$ in this panel. Fig. 2(c) shows the optimized sensitivity $\sqrt{T} \delta g_{\text{opt}}^s$ as a function of r at fixed $D/D_{\text{crit}}=0.2$, evaluated at the decoherence-limited optimal time $t_{\text{opt}}^{\text{dec}} \equiv \arg \min_t \sqrt{t/\mathcal{F}_Q(g,t)}$ (markers in inset). For $\gamma_0/\omega=10^{-4}$, the decoherent curve follows the coherent reference closely up to $r \approx r^*$, beyond which the sensitivity saturates rather than improving further. Larger γ_0 brings this saturation to smaller r , consistent with the crossover values identified in panel (a). Finally, Fig. 2(d) shows extracted $t_{\text{opt}}^{\text{dec}}$ as a function of r for the same γ_0 values, with the coherent reference $t_{\text{opt}}=\pi/\omega_b$ (dashed). The coherent time grows with r since ω_b decreases with squeezing. In the presence of damping, $t_{\text{opt}}^{\text{dec}}$ is pulled below this reference at all r , and the gap widens as either r or γ_0 increases. Together, panels (a)–(d) identify the practical operating window for the MSFQ gravimeter: increasing r raises Ξ , so the optimal squeezing for a given γ_0 is set by the condition $\Xi \lesssim 1$, i.e., $r \lesssim r^*(\gamma_0)$.

VI. CONCLUSION

In this paper, we propose a mechanical squeezed-Fock gravimeter in which gravity is sensed directly through the CM motion of a levitated mesoscopic particle. The protocol com-

bines the favorable mass scaling of quantized mechanical motion with the quadrature amplification generated by a detuned two-phonon pump. In the squeezed-Fock basis, the gravitational force couples to the anti-squeezed quadrature, enhancing the effective gravity-induced transition rate by a factor e^r while preserving the direct mechanical coupling to the particle mass. In the coherent regime and in the weak-force limit, the exact QFI results in $\sqrt{T} \delta g_{\text{opt}}^s \simeq e^{-r} \sqrt{\pi \hbar \omega \omega_b / 8m}$. This expression identifies the key resources of the sensor: squeezing-enhanced force coupling, large mechanical mass, and a tunably small qubit splitting ω_b . Increasing Duffing nonlinearity towards its allowed maximum improves sensitivity by reducing ω_b and simultaneously strengthens the anharmonic protection of the squeezed-qubit subspace. We also showed that population measurement in the squeezed-Fock basis saturates the QFI. We further analyzed the dissipative dynamics and showed that squeezing converts ordinary mechanical damping into anisotropic qubit noise. As a result, the optimal sensitivity is governed by a trade-off between signal amplification and decoherence. When the effective decoherence rate remains comparable with ω_b , the coherent advantage is largely retained; otherwise, the QFI is suppressed and the optimal interrogation time shifts to shorter values. In this noisy regime, the optimal measurement is determined by the SLD direction. Overall, our results establish the MSFQ as a promising platform for quantum gravimetry. The sensor preserves the direct CM coupling to gravity, enhances the signal through squeezing, and provides a clear operating window set by the balance between squeezing, anharmonic protection, interrogation time, and decoherence.

Appendix A: Effective Hamiltonian

This appendix derives the effective Hamiltonian used in the main text. Starting from

$$\hat{H}_{\text{rot}} = \hbar \delta \hat{a}^\dagger \hat{a} - \hbar D \hat{a}^\dagger \hat{a}^\dagger \hat{a} \hat{a} + \frac{\hbar A_p}{2} (e^{-i\theta} \hat{a}^2 + e^{i\theta} \hat{a}^{\dagger 2}) \quad (\text{A1})$$

we substitute the Bogoliubov transformation $\hat{a} = c \hat{b} - e^{i\theta} s \hat{b}^\dagger$, and $\hat{a}^\dagger = c \hat{b}^\dagger - e^{-i\theta} s \hat{b}$ in which $c \equiv \cosh r$, and $s \equiv \sinh r$, to simplify the Hamiltonian. First,

$$\hat{a}^\dagger \hat{a} = (c \hat{b}^\dagger - e^{-i\theta} s \hat{b}) (c \hat{b} - e^{i\theta} s \hat{b}^\dagger) = c^2 \hat{b}^\dagger \hat{b} - cs e^{i\theta} \hat{b}^\dagger \hat{b}^\dagger - cs e^{-i\theta} \hat{b} \hat{b} + s^2 \hat{b} \hat{b}^\dagger = (c^2 + s^2) \hat{b}^\dagger \hat{b} + s^2 - cs (e^{i\theta} \hat{b}^{\dagger 2} + e^{-i\theta} \hat{b}^2), \quad (\text{A2})$$

where we used $\hat{b} \hat{b}^\dagger = \hat{b}^\dagger \hat{b} + 1$. Next,

$$\hat{a}^2 = (c \hat{b} - e^{i\theta} s \hat{b}^\dagger)^2 = c^2 \hat{b}^2 - cs e^{i\theta} (\hat{b} \hat{b}^\dagger + \hat{b}^\dagger \hat{b}) + s^2 e^{i2\theta} \hat{b}^{\dagger 2}, \quad (\text{A3})$$

and similarly

$$\hat{a}^{\dagger 2} = c^2 \hat{b}^{\dagger 2} - cs e^{-i\theta} (\hat{b}^\dagger \hat{b} + \hat{b} \hat{b}^\dagger) + s^2 e^{-i2\theta} \hat{b}^2. \quad (\text{A4})$$

Therefore,

$$e^{-i\theta} \hat{a}^2 + e^{i\theta} \hat{a}^{\dagger 2} = (c^2 + s^2) (e^{-i\theta} \hat{b}^2 + e^{i\theta} \hat{b}^{\dagger 2}) - 2cs (2\hat{b}^\dagger \hat{b} + 1). \quad (\text{A5})$$

Substituting Eqs. (A2) and (A5) into the quadratic part of the Hamiltonian $\hat{H}_{\text{quad}} = \hbar \delta \hat{a}^\dagger \hat{a} + \frac{\hbar A_p}{2} (e^{-i\theta} \hat{a}^2 + e^{i\theta} \hat{a}^{\dagger 2})$, we obtain

$$\hat{H}_{\text{quad}} = \hbar \left[\delta (c^2 + s^2) - 2A_p c s \right] \hat{b}^\dagger \hat{b} + \hbar \left[\frac{A_p}{2} (c^2 + s^2) - \delta c s \right] (e^{-i\theta} \hat{b}^2 + e^{i\theta} \hat{b}^{\dagger 2}) + \hbar (\delta s^2 - A_p c s). \quad (\text{A6})$$

Using $c^2 + s^2 = \cosh 2r$ and $2cs = \sinh 2r$, the Eq. (A6) becomes

$$\hat{H}_{\text{quad}} = \hbar (\delta \cosh 2r - A_p \sinh 2r) \hat{b}^\dagger \hat{b} + \frac{\hbar}{2} (A_p \cosh 2r - \delta \sinh 2r) (e^{-i\theta} \hat{b}^2 + e^{i\theta} \hat{b}^{\dagger 2}) + \text{const.} \quad (\text{A7})$$

We choose the squeezing parameter r such that the anomalous terms vanish:

$$A_p \cosh 2r - \delta \sinh 2r = 0 \quad \implies \quad \tanh 2r = \frac{A_p}{\delta}. \quad (\text{A8})$$

With this choice, $\delta_b \equiv \delta \cosh 2r - A_p \sinh 2r = \sqrt{\delta^2 - A_p^2}$, and thus $\hat{H}_{\text{quad}} = \hbar \delta_b \hat{b}^\dagger \hat{b} + \text{const.}$

For the Duffing term

$$\hat{H}_D = -\hbar D \hat{a}^{\dagger 2} \hat{a}^2, \quad (\text{A9})$$

one has $\hat{a}^{\dagger 2} \hat{a}^2 = (c \hat{b}^\dagger - e^{-i\theta} s \hat{b})^2 (c \hat{b} - e^{i\theta} s \hat{b}^\dagger)^2$. After expanding this expression and repeatedly using the bosonic commutation relation $[\hat{b}, \hat{b}^\dagger] = 1$ to normal-order the operators, one finds

$$\begin{aligned} \hat{a}^{\dagger 2} \hat{a}^2 &= (8c^2 s^2 + 4s^4) \hat{b}^\dagger \hat{b} + \frac{3 \cosh 4r + 1}{4} \hat{b}^{\dagger 2} \hat{b}^2 \\ &+ \frac{\sinh^2 2r}{4} (e^{i2\theta} \hat{b}^{\dagger 4} + e^{-i2\theta} \hat{b}^4) - \frac{\sinh 4r}{2} (e^{i\theta} \hat{b}^{\dagger 3} \hat{b} + e^{-i\theta} \hat{b}^\dagger \hat{b}^3) + \frac{\sinh 2r (3 \cosh 2r - 2)}{2} (e^{i\theta} \hat{b}^{\dagger 2} + e^{-i\theta} \hat{b}^2) + \text{const.} \end{aligned} \quad (\text{A10})$$

Therefore,

$$\begin{aligned} \hat{H}_D &= -\hbar D (8c^2 s^2 + 4s^4) \hat{b}^\dagger \hat{b} - \hbar D \frac{3 \cosh 4r + 1}{4} \hat{b}^{\dagger 2} \hat{b}^2 \\ &- \hbar D \frac{\sinh^2 2r}{4} (e^{i2\theta} \hat{b}^{\dagger 4} + e^{-i2\theta} \hat{b}^4) + \hbar D \frac{\sinh 4r}{2} (e^{i\theta} \hat{b}^{\dagger 3} \hat{b} + e^{-i\theta} \hat{b}^\dagger \hat{b}^3) - \hbar D \frac{\sinh 2r (3 \cosh 2r - 2)}{2} (e^{i\theta} \hat{b}^{\dagger 2} + e^{-i\theta} \hat{b}^2) + \text{const.} \end{aligned} \quad (\text{A11})$$

Collecting all the above equations and dropping constant energy shifts, we get

$$\begin{aligned} \hat{H}_{\text{tot}} &= \hbar \omega_b \hat{b}^\dagger \hat{b} - \hbar U_b \hat{b}^{\dagger 2} \hat{b}^2 \\ &- \hbar D \frac{\sinh^2 2r}{4} (e^{i2\theta} \hat{b}^{\dagger 4} + e^{-i2\theta} \hat{b}^4) + \hbar D \frac{\sinh 4r}{2} (e^{i\theta} \hat{b}^{\dagger 3} \hat{b} + e^{-i\theta} \hat{b}^\dagger \hat{b}^3) - \hbar D \frac{\sinh 2r (3 \cosh 2r - 2)}{2} (e^{i\theta} \hat{b}^{\dagger 2} + e^{-i\theta} \hat{b}^2) \end{aligned} \quad (\text{A12})$$

where

$$\omega_b = \delta_b - D (8c^2 s^2 + 4s^4) = \sqrt{\delta^2 - A_p^2} - D (8 \cosh^2 r \sinh^2 r + 4 \sinh^4 r), \quad (\text{A13})$$

and

$$U_b = \frac{D}{4} (3 \cosh 4r + 1). \quad (\text{A14})$$

To apply the rotating-wave approximation, we move to the interaction picture with respect to

$$\hat{H}_0 = \hbar \omega_b \hat{b}^\dagger \hat{b}. \quad (\text{A15})$$

Therefore, $\hat{b}(t) = \hat{b} e^{-i\omega_b t}$, and $\hat{b}^\dagger(t) = \hat{b}^\dagger e^{i\omega_b t}$. This results in acquiring the rapid phases by the non-number-conserving quartic terms as

$$\begin{aligned} \hat{b}^{\dagger 4} &\rightarrow \hat{b}^{\dagger 4} e^{i4\omega_b t}, & \hat{b}^4 &\rightarrow \hat{b}^4 e^{-i4\omega_b t}, \\ \hat{b}^{\dagger 3} \hat{b} &\rightarrow \hat{b}^{\dagger 3} \hat{b} e^{i2\omega_b t}, & \hat{b}^\dagger \hat{b}^3 &\rightarrow \hat{b}^\dagger \hat{b}^3 e^{-i2\omega_b t}, \\ \hat{b}^{\dagger 2} &\rightarrow \hat{b}^{\dagger 2} e^{i2\omega_b t}, & \hat{b}^2 &\rightarrow \hat{b}^2 e^{-i2\omega_b t}. \end{aligned}$$

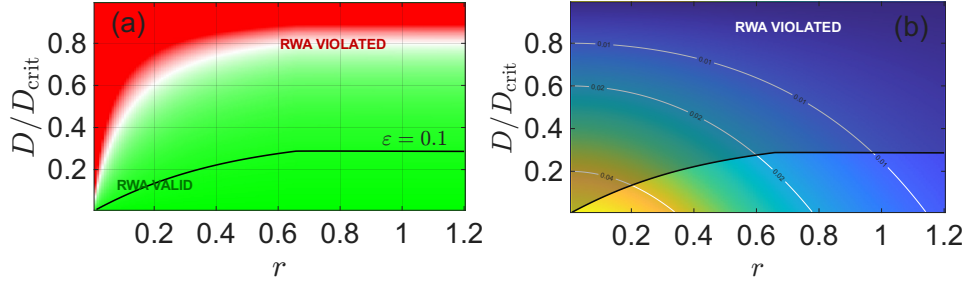


FIG. A1. (a) RWA validity; Largest of the three RWA condition ratios, $\max\left\{\frac{D \sinh^2(2r)}{16 \omega_b}, \frac{D \sinh(4r)}{4 \omega_b}, \frac{D \sinh(2r)(3 \cosh 2r - 2)}{4 \omega_b}\right\}$, in $(r, D/D_{\text{crit}})$ plane. The green (red) region marks where the RWA is valid (violated). (b) Rabi frequency ω_b/ω in $(r, D/D_{\text{crit}})$ plane. In both panels, the black contour defines the safe-operation boundary $D_{\text{RWA}}(r, \varepsilon, A_p)$ for $\varepsilon = 0.1$, obtained by simultaneously enforcing $D \sinh^2(2r)/4 < \varepsilon \cdot 4\omega_b$, $D \sinh(4r)/2 < \varepsilon \cdot 2\omega_b$, and $D \sinh(2r)(3 \cosh 2r - 2)/2 < \varepsilon \cdot 2\omega_b$. Both panels use $\delta/\omega = 0.05$.

When $D \frac{\sinh^2 2r}{4} \ll 4\omega_b$, $D \frac{\sinh 4r}{2} \ll 2\omega_b$, and $D \frac{\sinh 2r(3 \cosh 2r - 2)}{2} \ll 2\omega_b$, the above terms oscillate rapidly and can be neglected. Under this rotating-wave approximation (RWA), the effective Hamiltonian in the Schrödinger picture becomes

$$\hat{H}_{\text{eff}} \simeq \hbar \omega_b \hat{b}^\dagger \hat{b} - \hbar U_b \hat{b}^\dagger \hat{\sigma}^\dagger \hat{b} \hat{\sigma} \quad (\text{A16})$$

For each choice of the detuning δ and pump amplitude A_p , the squeezing parameter r is fixed by the ratio A_p/δ . Therefore, increasing A_p/δ increases r , which enhances the gravity-induced coupling. However, the same squeezing also reduces the effective qubit frequency ω_b . The shape of ω_b in Eq. (A13) obligates us to determine the boundary at which the qubit gap closes, namely $\omega_b=0$. As such we introduce $D_{\text{crit}} = \sqrt{\delta^2 - A_p^2} / (8 \cosh^2 r \sinh^2 r + 4 \sinh^4 r)$. Exactly at $D = D_{\text{crit}}$, the optimal interrogation time becomes infinitely long. To prevent this and the violation of the RWA, one should choose D safely below D_{crit} , where the squeezed-qubit picture remains valid and the sensing time is still finite. Fig. A1 maps the RWA validity conditions quantitatively. Fig. A1(a) displays the largest of the three condition ratios in the $(r, D/D_{\text{crit}})$ plane. The RWA is valid in the green region and violated in the red region. As r increases, the valid region shrinks rapidly, because the dropped terms grow as $\sinh(2r) \sim e^{2r}$ while ω_b simultaneously decreases. The black line defines $D_{\text{RWA}}(r, \varepsilon, A_p) < D_{\text{crit}}$ for $\varepsilon = 0.1$, when one enforces $D \frac{\sinh^2(2r)}{4} < \varepsilon \cdot 4\omega_b$, $D \frac{\sinh(4r)}{2} < \varepsilon \cdot 2\omega_b$, and $D \frac{\sinh(2r)(3 \cosh 2r - 2)}{2} < \varepsilon \cdot 2\omega_b$. Fig. A1(b) maps the renormalized Rabi frequency ω_b/ω over the entire $(r, D/D_{\text{crit}})$ plane. At fixed r , ω_b decreases monotonically with D/D_{crit} and vanishes at the critical boundary. At fixed D/D_{crit} , increasing r further suppresses ω_b through the squeezing-induced renormalization. Therefore, one must choose r and D small enough to keep the RWA valid and the qubit gap open, yet large enough to benefit from squeezing-enhanced signal amplification and reduced ω_b .

Appendix B: Coherent QFI and CFI

In this section we derive the coherent Fisher information used in the main text. The effective squeezed-qubit Hamiltonian is

$$\hat{H}_{\text{eff}}^s = \frac{\hbar \omega_b}{2} \hat{\sigma}_z + \frac{\hbar \Omega_g^s}{2} \hat{\sigma}_x. \quad (\text{B1})$$

For compactness, we write

$$\Omega \equiv \Omega_g^s, \quad \omega_R = \sqrt{\omega_b^2 + \Omega^2}, \quad \kappa_g \equiv \partial_g \Omega_g^s = \frac{2m x_0 e^r}{\hbar}. \quad (\text{B2})$$

Starting from $|0\rangle_s$, the evolved state is

$$|\psi(t)\rangle = \alpha(t)|0\rangle_s + \beta(t)|1\rangle_s, \quad (\text{B3})$$

with

$$\alpha(t) = \cos\left(\frac{\omega_R t}{2}\right) + i \frac{\omega_b}{\omega_R} \sin\left(\frac{\omega_R t}{2}\right), \quad (\text{B4})$$

$$\beta(t) = -i \frac{\Omega}{\omega_R} \sin\left(\frac{\omega_R t}{2}\right). \quad (\text{B5})$$

The pure-state QFI is

$$\mathcal{F}_Q(g) = 4 \left[\langle \partial_g \psi | \partial_g \psi \rangle - |\langle \psi | \partial_g \psi \rangle|^2 \right]. \quad (\text{B6})$$

Since g enters only through Ω , the chain rule gives

$$\mathcal{F}_Q(g) = \kappa_g^2 \mathcal{F}_Q(\Omega). \quad (\text{B7})$$

A direct calculation gives

$$\mathcal{F}_Q(g) = \kappa_g^2 \frac{\Omega^4 \omega_R^2 t^2 + 2\Omega^2 \omega_b^2 \omega_R t \sin(\omega_R t) + 4\omega_b^2 \omega_R^2 \sin^2\left(\frac{\omega_R t}{2}\right) - \Omega^2 \omega_b^2 \sin^2(\omega_R t)}{\omega_R^6}. \quad (\text{B8})$$

The population of the excited squeezed-Fock state is

$$P_1(t) = \frac{\Omega^2}{\omega_R^2} \sin^2\left(\frac{\omega_R t}{2}\right). \quad (\text{B9})$$

The CFI associated with the binary outcomes P_1 and $P_0 = 1 - P_1$ is

$$\mathcal{F}_C(g) = \frac{[\partial_g P_1(t)]^2}{P_1(t)[1 - P_1(t)]}. \quad (\text{B10})$$

Using

$$\partial_\Omega P_1 = \frac{2\Omega\omega_b^2}{\omega_R^4} \sin^2\left(\frac{\omega_R t}{2}\right) + \frac{\Omega^3 t}{2\omega_R^3} \sin(\omega_R t), \quad (\text{B11})$$

one obtains

$$\mathcal{F}_C(g) = \kappa_g^2 \frac{\left[\frac{2\Omega\omega_b^2}{\omega_R^4} \sin^2\left(\frac{\omega_R t}{2}\right) + \frac{\Omega^3 t}{2\omega_R^3} \sin(\omega_R t) \right]^2}{\frac{\Omega^2}{\omega_R^2} \sin^2\left(\frac{\omega_R t}{2}\right) \left[1 - \frac{\Omega^2}{\omega_R^2} \sin^2\left(\frac{\omega_R t}{2}\right) \right]}. \quad (\text{B12})$$

In the weak-force regime $\Omega \ll \omega_b$, Eqs. (B8) and (B12) reduce to

$$\mathcal{F}_Q(g) \simeq \mathcal{F}_C(g) \simeq \kappa_g^2 \frac{4}{\omega_b^2} \sin^2\left(\frac{\omega_b t}{2}\right) = \frac{8me^{2r}}{\hbar\omega\omega_b^2} \sin^2\left(\frac{\omega_b t}{2}\right). \quad (\text{B13})$$

Appendix C: Decoherence: master-equation solution and Fisher information

We now include mechanical damping in the squeezed-qubit subspace. The zero-temperature damping channel of the original mechanical mode is

$$\dot{\rho} = -\frac{i}{\hbar} [\hat{H}, \rho] + \frac{\gamma_0}{2} \mathcal{D}_{\hat{a}, \hat{a}^\dagger}[\rho]. \quad (\text{C1})$$

Using

$$\hat{a} = \cosh r \hat{b} - e^{i\theta} \sinh r \hat{b}^\dagger, \quad (\text{C2})$$

and projecting onto the squeezed-qubit subspace gives

$$\hat{a} \rightarrow \hat{L}_s = \cosh r \hat{\sigma}_- - e^{i\theta} \sinh r \hat{\sigma}_+. \quad (\text{C3})$$

For the sensing phase $\theta = \pi$, this becomes

$$\hat{L}_s = c \hat{\sigma}_- + s \hat{\sigma}_+, \quad c \equiv \cosh r, \quad s \equiv \sinh r. \quad (\text{C4})$$

The projected master equation is therefore

$$\dot{\rho} = -\frac{i}{2}[\omega_b \hat{\sigma}_z + \Omega \hat{\sigma}_x, \rho] + \frac{\gamma_0}{2} \mathcal{D}_{\hat{L}_s, \hat{L}_s^\dagger}[\rho], \quad (\text{C5})$$

where $\Omega \equiv \Omega_g^s$. Expanding the dissipator gives

$$\begin{aligned} \frac{\gamma_0}{2} \mathcal{D}_{\hat{L}_s, \hat{L}_s^\dagger}[\rho] &= \frac{\gamma_0}{2} c^2 \mathcal{D}_{\hat{\sigma}_-, \hat{\sigma}_+}[\rho] + \frac{\gamma_0}{2} s^2 \mathcal{D}_{\hat{\sigma}_+, \hat{\sigma}_-}[\rho] \\ &\quad + \gamma_0 c s (\hat{\sigma}_- \rho \hat{\sigma}_- + \hat{\sigma}_+ \rho \hat{\sigma}_+). \end{aligned} \quad (\text{C6})$$

The first term is relaxation, the second term is excitation induced by the squeezed representation of the bath, and the last line is the phase-sensitive contribution. To solve Eq. (C5), write the density matrix as

$$\rho(t) = \frac{1}{2} [\mathbb{1} + x(t) \hat{\sigma}_x + y(t) \hat{\sigma}_y + z(t) \hat{\sigma}_z], \quad \mathbf{v}(t) = \begin{pmatrix} x(t) \\ y(t) \\ z(t) \end{pmatrix}. \quad (\text{C7})$$

Using $\hat{\sigma}_z = |1\rangle_{ss}\langle 1| - |0\rangle_{ss}\langle 0|$, the initial state $|0\rangle_s$ corresponds to

$$\mathbf{v}(0) = \begin{pmatrix} 0 \\ 0 \\ -1 \end{pmatrix}. \quad (\text{C8})$$

Equation (C5) is equivalent to

$$\dot{\mathbf{v}}(t) = \mathbf{A}(\Omega) \mathbf{v}(t) + \mathbf{b}, \quad (\text{C9})$$

with

$$\mathbf{A}(\Omega) = \begin{pmatrix} -\Gamma_x & \omega_b & 0 \\ -\omega_b & -\Gamma_y & \Omega \\ 0 & -\Omega & -\Gamma_z \end{pmatrix}, \quad \mathbf{b} = \begin{pmatrix} 0 \\ 0 \\ -\gamma_0 \end{pmatrix}, \quad (\text{C10})$$

where

$$\Gamma_x = \frac{\gamma_0}{2}(c-s)^2 = \frac{\gamma_0}{2} e^{-2r}, \quad \Gamma_y = \frac{\gamma_0}{2}(c+s)^2 = \frac{\gamma_0}{2} e^{2r}, \quad \Gamma_z = \gamma_0(c^2 + s^2) = \gamma_0 \cosh(2r). \quad (\text{C11})$$

The exact solution is

$$\mathbf{v}(t) = \mathbf{v}_{ss} + \exp[\mathbf{A}(\Omega)t] [\mathbf{v}(0) - \mathbf{v}_{ss}], \quad (\text{C12})$$

where

$$\mathbf{v}_{ss} = -\mathbf{A}(\Omega)^{-1} \mathbf{b}. \quad (\text{C13})$$

This is the closed-form solution of the master equation; the exponential of the 3×3 matrix gives the full damped Rabi dynamics for arbitrary Ω , ω_b , r , and γ_0 within the squeezed-qubit approximation.

For the Fisher information, we need the derivative of $\mathbf{v}(t)$ with respect to Ω . Instead of differentiating Eq. (C12) explicitly, it is cleaner to propagate the sensitivity vector

$$\mathbf{u}(t) \equiv \partial_\Omega \mathbf{v}(t). \quad (\text{C14})$$

Differentiating Eq. (C9) gives

$$\dot{\mathbf{u}}(t) = \mathbf{A}(\Omega) \mathbf{u}(t) + \mathbf{A}_\Omega \mathbf{v}(t), \quad \mathbf{u}(0) = 0, \quad (\text{C15})$$

where

$$\mathbf{A}_\Omega \equiv \partial_\Omega \mathbf{A} = \begin{pmatrix} 0 & 0 & 0 \\ 0 & 0 & 1 \\ 0 & -1 & 0 \end{pmatrix}. \quad (\text{C16})$$

Equivalently,

$$\mathbf{u}(t) = \int_0^t \exp[\mathbf{A}(\Omega)(t - \tau)] \mathbf{A}_\Omega \mathbf{v}(\tau) d\tau. \quad (\text{C17})$$

The derivative with respect to g is then

$$\partial_g \mathbf{v}(t) = \kappa_g \mathbf{u}(t), \quad \kappa_g = \frac{2m\chi_0 e^f}{\hbar}. \quad (\text{C18})$$

For a mixed qubit state with Bloch vector \mathbf{v} , the QFI with respect to g is

$$\mathcal{F}_Q^{\text{dec}}(g) = |\partial_g \mathbf{v}|^2 + \frac{(\mathbf{v} \cdot \partial_g \mathbf{v})^2}{1 - |\mathbf{v}|^2}. \quad (\text{C19})$$

Using $\partial_g \mathbf{v} = \kappa_g \mathbf{u}$, this becomes

$$\boxed{\mathcal{F}_Q^{\text{dec}}(g) = \kappa_g^2 \left[\mathbf{u} \cdot \mathbf{u} + \frac{(\mathbf{v} \cdot \mathbf{u})^2}{1 - \mathbf{v} \cdot \mathbf{v}} \right]}. \quad (\text{C20})$$

The population measurement in the squeezed-Fock basis, $\{|0\rangle_s, |1\rangle_s\}$, is not generally the optimal measurement in the presence of decoherence. To quantify the maximum classical information that can be extracted by a qubit projective measurement, we consider a general readout axis \mathbf{n} on the Bloch sphere, with projectors

$$\Pi_{\pm}^{(\mathbf{n})} = \frac{1}{2} (\mathbb{I} \pm \mathbf{n} \cdot \boldsymbol{\sigma}), \quad |\mathbf{n}| = 1. \quad (\text{C21})$$

Writing the density matrix as

$$\rho(t) = \frac{1}{2} [\mathbb{I} + \mathbf{v}(t) \cdot \boldsymbol{\sigma}], \quad (\text{C22})$$

the outcome probabilities are

$$P_{\pm}^{(\mathbf{n})} = \frac{1}{2} [1 \pm \mathbf{n} \cdot \mathbf{v}(t)]. \quad (\text{C23})$$

The corresponding classical Fisher information is therefore

$$\mathcal{F}_C^{(\mathbf{n})}(g) = \frac{[\mathbf{n} \cdot \mathbf{u}(t)]^2}{1 - [\mathbf{n} \cdot \mathbf{v}(t)]^2}. \quad (\text{C24})$$

The conventional population measurement corresponds to $\mathbf{n} = \hat{\mathbf{z}}$, namely

$$\mathcal{F}_C^{(\hat{\mathbf{z}})}(g) = \frac{u_z^2(t)}{1 - z^2(t)}. \quad (\text{C25})$$

The optimized readout is obtained by choosing the measurement axis along the symmetric-logarithmic-derivative direction. For a mixed qubit state this direction is

$$\mathbf{n}_{\text{opt}} = \frac{\boldsymbol{\ell}}{|\boldsymbol{\ell}|}, \quad \boldsymbol{\ell} = \mathbf{u} + \frac{\mathbf{v} \cdot \mathbf{u}}{1 - |\mathbf{v}|^2} \mathbf{v}. \quad (\text{C26})$$

We parameterize this axis by the polar and azimuthal angles

$$\mathbf{n}_{\text{opt}} = (\sin \theta_{\text{opt}} \cos \phi_{\text{opt}}, \sin \theta_{\text{opt}} \sin \phi_{\text{opt}}, \cos \theta_{\text{opt}}), \quad (\text{C27})$$

with

$$\theta_{\text{opt}} = \arccos(n_z), \quad \phi_{\text{opt}} = \text{atan2}(n_y, n_x). \quad (\text{C28})$$

The optimized-readout CFI is then

$$\mathcal{F}_C^{\text{opt}}(g) = \frac{[\mathbf{n}_{\text{opt}} \cdot \mathbf{u}(t)]^2}{1 - [\mathbf{n}_{\text{opt}} \cdot \mathbf{v}(t)]^2}. \quad (\text{C29})$$

This construction gives the best CFI obtainable from a two-outcome projective measurement at the chosen operating point. Physically, this means that decoherence can rotate or redistribute the information about g among the Bloch-vector components. A fixed population measurement extracts only the z -component of this information, whereas the optimized readout measures along the direction in which the state changes most sensitively with respect to g . Experimentally, such a readout can be implemented by applying a final qubit rotation that maps $\mathbf{n}_{\text{opt}} \cdot \boldsymbol{\sigma}$ onto σ_z , followed by the usual population measurement. Figure C1 displays the locally optimal projective readout used to obtain the optimized CFI in the decoherent calculations.

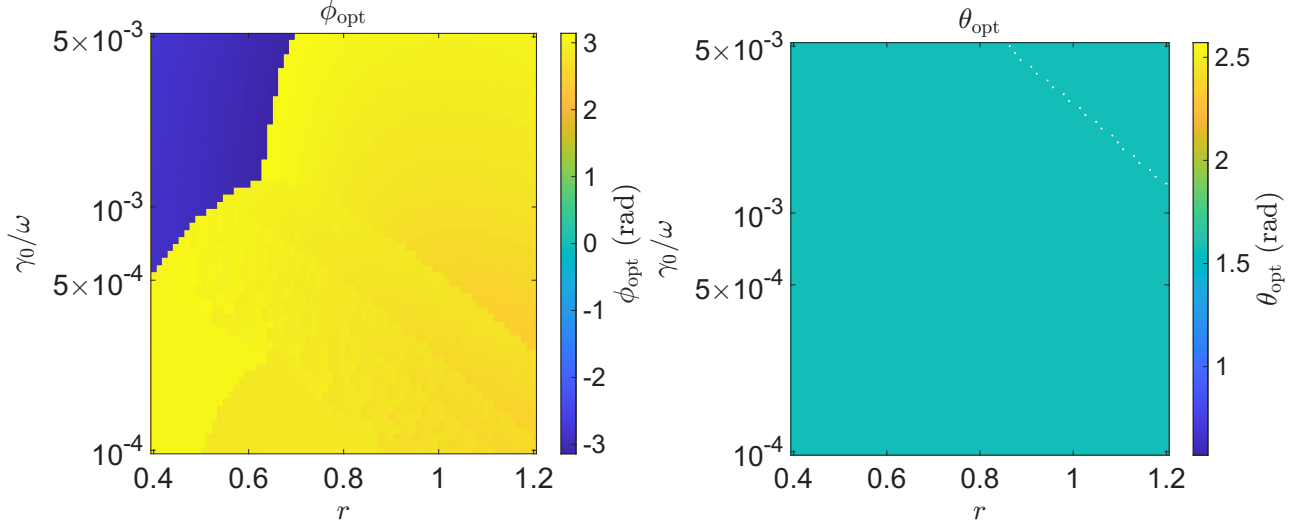


FIG. C1. Corresponding optimal angles θ_{opt} and ϕ_{opt} in $(\gamma_0/\omega, r)$ plane, that determine the locally optimal readout direction $\mathbf{n}_{\text{opt}} = (\sin \theta_{\text{opt}} \cos \phi_{\text{opt}}, \sin \theta_{\text{opt}} \sin \phi_{\text{opt}}, \cos \theta_{\text{opt}})$ for the decoherent MSF gravimeter.

-
- [1] B. Stray, A. Lamb, A. Kaushik, J. Vovrosh, A. Rodgers, J. Winch, F. Hayati, D. Boddice, A. Stabrawa, A. Niggebaum, M. Langlois, Y.-H. Lien, S. Lellouch, S. Roshanmanesh, K. Ridley, G. de Villiers, G. Brown, T. Cross, G. Tuckwell, A. Faramarzi, N. Metje, K. Bongs, and M. Holynski, Quantum sensing for gravity cartography, *Nature* **602**, 590 (2022).
 - [2] S. E. Crawford, G. R. Lander, H. P. Paudel, M. R. Slot, N. Lalam, J. Wuenschell, R. Pingree, R. Oueid, R. Wright, M. Buric, M. M. Brister, and Y. Duan, Quantum sensing for emerging energy technologies, *Nat. Rev. Clean Technol.* **1**, 861 (2025).
 - [3] F. Forster, A. Güntner, P. Jousset, M. Reich, B. Männel, J. Hinderer, and K. Erbas, Environmental and anthropogenic gravity contributions at the theistareykir geothermal field, north Iceland, *Geothermal Energy* **9**, 26 (2021).
 - [4] X. Wu, Z. Pagel, B. S. Malek, T. H. Nguyen, F. Zi, D. S. Scheirer, and H. Müller, Gravity surveys using a mobile atom interferometer, *Science Advances* **5**, eaax0800 (2019).
 - [5] M. Krelina, Quantum technology for military applications, *EPJ Quantum Technol.* **8**, 24 (2021).
 - [6] J. Ye and P. Zoller, Essay: Quantum sensing with atomic, molecular, and optical platforms for fundamental physics, *Phys. Rev. Lett.* **132**, 190001 (2024).
 - [7] N. Poli, F.-Y. Wang, M. G. Tarallo, A. Alberti, M. Prevedelli, and G. M. Tino, Precision measurement of gravity with cold atoms in an optical lattice and comparison with a classical gravimeter, *Phys. Rev. Lett.* **106**, 038501 (2011).
 - [8] M. Kasevich and S. Chu, Atomic interferometry using stimulated Raman transitions, *Phys. Rev. Lett.* **67**, 181 (1991).
 - [9] A. Peters, K. Y. Chung, and S. Chu, Measurement of gravitational acceleration by dropping atoms, *Nature* **400**, 849 (1999).
 - [10] R. Geiger, A. Landragin, S. Merlet, and F. Pereira Dos Santos, High-accuracy inertial measurements with cold-atom sensors, *AVS Quantum Science* **2**, 024702 (2020).
 - [11] J. Wei, J. Huang, and C. Lee, Adaptive robust high-precision atomic gravimetry, *Phys. Rev. Res.* **7**, L012064 (2025).
 - [12] Y. Bidet, N. Zahzam, C. Blanchard, A. Bonnin, M. Cadoret, A. Bresson, D. Rouxel, and M. F. Lequentrec-Lalancette, Absolute marine gravimetry with matter-wave interferometry, *Nat. Commun.* **9**, 627 (2018).

- [13] Z.-K. Hu, B.-L. Sun, X.-C. Duan, M.-K. Zhou, L.-L. Chen, S. Zhan, Q.-Z. Zhang, and J. Luo, Demonstration of an ultrahigh-sensitivity atom-interferometry absolute gravimeter, *Phys. Rev. A* **88**, 043610 (2013).
- [14] V. Ménot, P. Vermeulen, N. Le Moigne, S. Bonvalot, P. Bouyer, A. Landragin, and B. Desruelle, Gravity measurements below 10^{-9} g with a transportable absolute quantum gravimeter, *Sci. Rep.* **8**, 12300 (2018).
- [15] T. Zhang, L.-L. Chen, Y.-B. Shu, W.-J. Xu, Y. Cheng, Q. Luo, Z.-K. Hu, and M.-K. Zhou, Ultrahigh-sensitivity bragg atom gravimeter and its application in testing lorentz violation, *Phys. Rev. Applied* **20**, 014067 (2023).
- [16] A. Peters, K. Y. Chung, and S. Chu, High-precision gravity measurements using atom interferometry, *Metrologia* **38**, 25 (2001).
- [17] J. Le Gouët, T. E. Mehlstäubler, J. Kim, S. Merlet, A. Clairon, A. Landragin, and F. Pereira Dos Santos, Limits to the sensitivity of a low noise compact atomic gravimeter, *Appl. Phys. B* **92**, 133 (2008).
- [18] S. Merlet, J. Le Gouët, Q. Bodart, A. Clairon, A. Landragin, F. Pereira Dos Santos, and P. Rouchon, Operating an atom interferometer beyond its linear range, *Metrologia* **46**, 87 (2009).
- [19] M.-K. Zhou, Z.-K. Hu, X.-C. Duan, B.-L. Sun, L.-L. Chen, Q.-Z. Zhang, and J. Luo, Performance of a cold-atom gravimeter with an active vibration isolator, *Phys. Rev. A* **86**, 043630 (2012).
- [20] M. Rademacher, J. Millen, and Y. L. Li, Quantum sensing with nanoparticles for gravimetry: when bigger is better, *Adv. Opt. Technol.* **9**, 227 (2020).
- [21] C. Gonzalez-Ballester, M. Aspelmeyer, L. Novotny, R. Quidant, and O. Romero-Isart, Levitodynamics: levitation and control of microscopic objects in vacuum, *Science* **374**, eabg3027 (2021).
- [22] S. Bose, I. Fuentes, A. A. Geraci, S. M. Khan, S. Qvarfort, M. Rademacher, M. Rashid, M. Toroš, H. Ulbricht, and C. C. Wanjura, Massive quantum systems as interfaces of quantum mechanics and gravity, *Rev. Mod. Phys.* **97**, 015003 (2025).
- [23] L. Dania, D. S. Bykov, F. Goschin, M. Teller, A. Kassid, and T. E. Northup, Ultrahigh quality factor of a levitated nanomechanical oscillator, *Phys. Rev. Lett.* **132**, 133602 (2024).
- [24] X.-W. Huo, J.-H. An, and P.-B. Li, Quantum gravimetry with mechanical qubits (2026), arXiv:2604.14950 [quant-ph].
- [25] U. Delić, M. Reisenbauer, K. Dare, D. Grass, V. Vuletić, N. Kiesel, and M. Aspelmeyer, Cooling of a levitated nanoparticle to the motional quantum ground state, *Science* **367**, 892 (2020).
- [26] F. Tebbenjohanns, M. L. Mattana, M. Rossi, M. Frimmer, and L. Novotny, Quantum control of a nanoparticle optically levitated in cryogenic free space, *Nature* **595**, 378 (2021).
- [27] L. Magrini, P. Rosenzweig, C. Bach, A. Deutschmann-Olek, S. G. Hofer, S. Hong, N. Kiesel, A. Kugi, and M. Aspelmeyer, Real-time optimal quantum control of mechanical motion at room temperature, *Nature* **595**, 373 (2021).
- [28] M. Kamba, R. Shimizu, and K. Aikawa, Quantum squeezing of a levitated nanomechanical oscillator, *Science* **389**, 1225 (2025).
- [29] S. Marti, U. von Lüpke, O. Joshi, Y. Yang, M. Bild, A. Omani, Y. Chu, and M. Fadel, Quantum squeezing in a nonlinear mechanical oscillator, *Nat. Phys.* **20**, 1448 (2024).
- [30] J. Piotrowski, D. Windey, J. Vijayan, C. Gonzalez-Ballester, A. de los Ríos Sommer, N. Altundaš, A. Blais, O. Romero-Isart, R. Quidant, and U. Delić, Simultaneous ground-state cooling of two mechanical modes of a levitated nanoparticle, *Nat. Phys.* **19**, 1009 (2023).
- [31] M. Scala, M. S. Kim, G. W. Morley, P. F. Barker, and S. Bose, Matter-wave interferometry of a levitated thermal nano-oscillator induced and probed by a spin, *Phys. Rev. Lett.* **111**, 180403 (2013).
- [32] L.-Y. Wang, J.-F. Wei, K.-F. Cui, S.-L. Su, L.-L. Yan, H.-Z. Guo, C.-X. Shan, and G. Chen, Enhanced gravity sensing by a levitated mesoscopic nanoparticle, *Phys. Rev. Lett.* **135**, 120803 (2025).
- [33] S. Qvarfort, A. Serafini, P. F. Barker, and S. Bose, Gravimetry through non-linear optomechanics, *Nat. Commun.* **9**, 3690 (2018).
- [34] P.-B. Li, Y. Zhou, W.-B. Gao, and F. Nori, Enhancing spin-phonon and spin-spin interactions using linear resources in a hybrid quantum system, *Phys. Rev. Lett.* **125**, 153602 (2020).
- [35] P.-B. Li, Z.-L. Xiang, P. Rabl, and F. Nori, Hybrid quantum device with nitrogen-vacancy centers in diamond coupled to carbon nanotubes, *Phys. Rev. Lett.* **117**, 015502 (2016).
- [36] S. Rips and M. J. Hartmann, Quantum information processing with nanomechanical qubits, *Phys. Rev. Lett.* **110**, 120503 (2013).
- [37] F. Pistolesi, A. N. Cleland, and A. Bachtold, Proposal for a nanomechanical qubit, *Phys. Rev. X* **11**, 031027 (2021).
- [38] C. Samanta, S. L. De Bonis, C. B. Møller, R. Tormo-Queralt, W. Yang, C. Urgell, B. Stamenic, B. Thibeault, Y. Jin, D. A. Czaplewski, F. Pistolesi, and A. Bachtold, Nonlinear nanomechanical resonators approaching the quantum ground state, *Nat. Phys.* **19**, 1340 (2023).
- [39] P. Sharma, J. Koch, and E. Ginossar, Towards a micromechanical qubit based on quantized oscillations in superfluid helium (2025), arXiv:2409.02028.
- [40] S. Savel'ev, X. Hu, and F. Nori, Quantum electromechanics: Qubits from buckling nanobars, *New J. Phys.* **8**, 105 (2006).
- [41] S. Savel'ev, A. L. Rakhmanov, X. Hu, A. Kasumov, and F. Nori, Quantum electromechanics: Quantum tunneling near resonance and qubits from buckling nanobars, *Phys. Rev. B* **75**, 165417 (2007).
- [42] S. Rips, I. Wilson-Rae, and M. J. Hartmann, Nonlinear nanomechanical resonators for quantum optoelectromechanics, *Phys. Rev. A* **89**, 013854 (2014).
- [43] C. Flühmann, T. L. Nguyen, M. Marinelli, V. Negnevitsky, K. Mehta, and J. P. Home, Encoding a qubit in a trapped-ion mechanical oscillator, *Nature* **566**, 513 (2019).
- [44] Y. Yang, I. Kladarić, M. Drimmer, U. von Lüpke, D. Lenterman, J. Bus, S. Marti, M. Fadel, and Y. Chu, A mechanical qubit, *Science* **386**, 783 (2024).
- [45] F. Pistolesi, The journey to a mechanical qubit, *Science* **386**, 728 (2024).
- [46] Y.-F. Qiao, J.-H. An, and P.-B. Li, Mechanical squeezed-fock qubit: Towards quantum weak-force sensing, *Phys. Rev. Lett.* **136**, 040801 (2026).
- [47] C. W. Helstrom, Quantum detection and estimation theory, *J. Stat. Phys.* **1**, 231 (1969).
- [48] M. G. A. Paris, Quantum estimation for quantum technology, *Int. J. Quantum Inf.* **7**, 125 (2009).
- [49] V. Montenegro, C. Mukhopadhyay, R. Yousefjani, S. Sarkar, U. Mishra, M. G. A. Paris, and A. Bayat, Review: Quantum metrology and sensing with many-body systems, *Phys. Rep.* **1134**, 1 (2025).
- [50] S. L. Braunstein and C. M. Caves, Statistical distance and the geometry of quantum states, *Phys. Rev. Lett.* **72**, 3439 (1994).
- [51] C. W. Gardiner and P. Zoller, *Quantum Noise: A Handbook of Markovian and Non-Markovian Quantum Stochastic Methods with Applications to Quantum Optics*, 3rd ed. (Springer, Berlin, 2004).

- [52] H.-P. Breuer and F. Petruccione, *The Theory of Open Quantum Systems* (Oxford University Press, Oxford, 2002).
- [53] M. Aspelmeyer, T. J. Kippenberg, and F. Marquardt, Cavity optomechanics, *Rev. Mod. Phys.* **86**, 1391 (2014).
- [54] A. A. Clerk, M. H. Devoret, S. M. Girvin, F. Marquardt, and R. J. Schoelkopf, Introduction to quantum noise, measurement, and amplification, *Rev. Mod. Phys.* **82**, 1155 (2010).
- [55] R. Fazio, J. Keeling, L. Mazza, and M. Schirò, Many-body open quantum systems, *SciPost Physics Lecture Notes* **99**, 10.21468/SciPostPhysLectNotes.99 (2025).